J. Fluid Mech. (1972), *vol.* 56, *part* 2, *pp.* 265–276
Printed in Great Britain

Numerical calculation of internal wave motions

By JAMES A. YOUNG
Science Applications, Inc., La Jolla, California
AND C. W. HIRT
University of California, Los Alamos Scientific Laboratory, Los Alamos, New Mexico

(Received 1 March 1972 and in revised form 1 August 1972)

A finite-difference technique for the numerical calculation of two-dimensional stratified incompressible fluid flows is presented. Small density variations are not assumed, so that this method is generally applicable to a wide variety of problems. To illustrate this new technique a calculation has been made of the collapse of a uniformly mixed region in a linearly stratified fluid. In addition to giving excellent agreement with experimental data, the calculations also reveal the mechanism for an observed change in scaling behaviour.

1. Introduction

With the advent of high-speed computers it is now possible to perform numerical calculations for quite complex hydrodynamic phenomena. In this paper we report a method capable of computing internal wave motion for a great variety of physical situations. Briefly, the computer is programmed to solve the complete set of Navier–Stokes equations for an incompressible stratified fluid. The basic method is the Marker-and-Cell (MAC) method developed by Harlow and others (see Harlow & Welch 1965; Amsden & Harlow 1970), suitably changed and improved to suit the task at hand. The principal improvements from the original MAC approach lie in the variable-density and free-surface treatments.

As an important application, as well as test, of the method, we have performed a numerical simulation of an experiment of Wu (1969) involving the collapse of a uniformly mixed region imbedded in a linearly stratified fluid. The agreement between theory and experiment is excellent. In addition the calculation offers an explanation for a change in scaling behaviour observed by Wu.

In § 2 a brief discussion of the computation method is given, followed in § 3 by a description of the comparison between calculation and experiment.

2. The computational method

In this section we briefly mention the numerical methods employed, giving details only where they have either been changed from or improved over previously reported work. Our code SAPHIRE is two-dimensional and employs Cartesian geometry. The basic numerical technique used in SAPHIRE, for the integration of the Navier–Stokes equations, is the MAC FORTRAN code listed

in Amsden & Harlow (1970). This is an Eulerian finite-difference technique using massless marker particles to define the free-surface position. The difference equations are explicit, being first-order in time and second-order in space. Velocities are defined on the faces of a network of rectangular cells while pressures and densities are defined at cell centres. For completeness, we present here the momentum difference equations used in MAC:

$$
\begin{aligned}
(\rho u)^{n+1}_{i+\frac{1}{2},j} = (\rho u)_{i+\frac{1}{2},j} + \delta t \Bigg[& \frac{(\rho u^2)_{i,j} - (\rho u^2)_{i+1,j}}{\delta x} + \frac{(\rho uv)_{i+\frac{1}{2},j-\frac{1}{2}} - (\rho uv)_{i+\frac{1}{2},j+\frac{1}{2}}}{\delta y} \\
& + 2\frac{\mu_{i+1,j}(u_{i+\frac{3}{2},j} - u_{i+\frac{1}{2},j}) - \mu_{i,j}(u_{i+\frac{1}{2},j} - u_{i-\frac{1}{2},j})}{\delta x^2} \\
& + \frac{\mu_{i+\frac{1}{2},j+\frac{1}{2}}}{\delta y}\left(\frac{u_{i+\frac{1}{2},j+1} - u_{i+\frac{1}{2},j}}{\delta y} + \frac{v_{i+1,j+\frac{1}{2}} - v_{i,j+\frac{1}{2}}}{\delta x}\right) \\
& - \frac{\mu_{i+\frac{1}{2},j-\frac{1}{2}}}{\delta y}\left(\frac{u_{i+\frac{1}{2},j} - u_{i+\frac{1}{2},j-1}}{\delta y} + \frac{v_{i+1,j-\frac{1}{2}} - v_{i,j-\frac{1}{2}}}{\delta x}\right) \\
& + \rho_{i+\frac{1}{2},j} g_x + \frac{p^{n+1}_{i,j} - p^{n+1}_{i+1,j}}{\delta x}\Bigg],
\end{aligned}
\tag{2.1}
$$

$$
\begin{aligned}
(\rho v)^{n+1}_{i,j+\frac{1}{2}} = (\rho v)_{i,j+\frac{1}{2}} + \delta t \Bigg[& \frac{(\rho uv)_{i-\frac{1}{2},j+\frac{1}{2}} - (\rho uv)_{i+\frac{1}{2},j+\frac{1}{2}}}{\delta x} + \frac{(\rho v^2)_{i,j} - (\rho v^2)_{i,j+1}}{\delta y} \\
& + 2\frac{\mu_{i,j+1}(v_{i,j+\frac{3}{2}} - v_{i,j+\frac{1}{2}}) - \mu_{i,j}(v_{i,j+\frac{1}{2}} - v_{i,j-\frac{1}{2}})}{\delta y^2} \\
& + \frac{\mu_{i+\frac{1}{2},j+\frac{1}{2}}}{\delta x}\left(\frac{u_{i+\frac{1}{2},j+1} - u_{i+\frac{1}{2},j}}{\delta y} + \frac{v_{i+1,j+\frac{1}{2}} - v_{i,j+\frac{1}{2}}}{\delta x}\right) \\
& - \frac{\mu_{i-\frac{1}{2},j+\frac{1}{2}}}{\delta x}\left(\frac{u_{i-\frac{1}{2},j+1} - u_{i-\frac{1}{2},j}}{\delta y} + \frac{v_{i,j+\frac{1}{2}} - v_{i-1,j+\frac{1}{2}}}{\delta x}\right) \\
& + \rho_{i,j+\frac{1}{2}} g_y + \frac{p^{n+1}_{i,j} - p^{n+1}_{i,j+1}}{\delta y}\Bigg].
\end{aligned}
\tag{2.2}
$$

Here u and v are the x and y components of the fluid velocity $\mathbf{u}$, ρ is the density, μ the viscosity and δt the time increment. The subscripts i and j refer to the mesh points in the x and y directions respectively. Gravity is denoted by the vector $\mathbf{g}$, and the superscript $n+1$ refers to the $(n+1)$th time step. The label n for the time step (cycle) is omitted except on the pressure terms. It should be noted that all quantities on the right-hand side of (2.1) and (2.2) except pressures, are evaluated at the time level n.

It is necessary to have a difference equation for the density changes if one wishes to compute the flow of a stratified fluid. Previous numerical calculations by Wessel (1969) for incompressible stratified flow have employed the Boussinesq approximation, but here we compute all the effects of density changes directly. The equation of continuity is

$$\partial\rho/\partial t + \nabla.(\rho\mathbf{u}) = 0, \tag{2.3}$$

while the incompressibility condition is

$$D\rho/Dt = 0 = \partial\rho/\partial t + \mathbf{u}.\nabla\rho = 0. \tag{2.4}$$

It has been assumed that the diffusion of the solute producing the stratification we wish to study is insignificant on the time scales of interest, otherwise diffusion terms are needed in the right-hand sides of (2.3) and (2.4).

One could, in principle, use either (2.3) or (2.4) to advance the density field. We prefer the former because it exactly satisfies mass conservation when written in finite-difference form. The condition for incompressibility is satisfied by requiring that $\nabla . \mathbf{u} = 0$. This is accomplished, as in the original MAC method, by calculating the pressure needed at time step $n+1$, for use in (2.1) and (2.2), from the requirement that $\nabla . \mathbf{u} = 0$ at step $n+1$ for each cell in the mesh. The resulting equation for the pressures is

$$p_{i,j}^{n+1} = \left[\frac{1}{\delta x^2}\left(\frac{1}{\rho_{i+\frac{1}{2},j}^{n+1}} + \frac{1}{\rho_{i-\frac{1}{2},j}^{n+1}}\right) + \frac{1}{\delta y^2}\left(\frac{1}{\rho_{i,j+\frac{1}{2}}^{n+1}} + \frac{1}{\rho_{i,j-\frac{1}{2}}^{n+1}}\right)\right]^{-1}$$
$$\times \left[-\frac{\tilde{D}_{i,j}^{n+1}}{\delta t} + \frac{1}{\delta x^2}\left(\frac{p_{i+1,j}^{n+1}}{\rho_{i+\frac{1}{2},j}^{n+1}} + \frac{p_{i-1,j}^{n+1}}{\rho_{i-\frac{1}{2},j}^{n+1}}\right) + \frac{1}{\delta y^2}\left(\frac{p_{i,j+1}^{n+1}}{\rho_{i,j+\frac{1}{2}}^{n+1}} + \frac{p_{i,j-1}^{n+1}}{\rho_{i,j-\frac{1}{2}}^{n+1}}\right)\right], \tag{2.5}$$

where $\tilde{D}_{i,j}$ is just the finite-difference form of $\nabla . \tilde{\mathbf{u}}$ (given below) and the velocities $\tilde{u}$ and $\tilde{v}$ are defined by (2.1), (2.2) and

$$u_{i+\frac{1}{2},j}^{n+1} = \tilde{u}_{i+\frac{1}{2},j}^{n+1} - \frac{\delta t}{\rho_{i+\frac{1}{2},j}^{n+1}\delta x}(p_{i+1,j}^{n+1} - p_{i,j}^{n+1}),$$

$$v_{i,j+\frac{1}{2}}^{n+1} = \tilde{v}_{i,j+\frac{1}{2}}^{n+1} - \frac{\delta t}{\rho_{i,j+\frac{1}{2}}^{n+1}\delta y}(p_{i,j+1}^{n+1} - p_{i,j}^{n+1}).$$

Equation (2.5) is solved for $p_{i,j}^{n+1}$ by a relaxation technique.

From (2.3), the expression to be used for advancing the density field from cycle n to cycle $n+1$ is

$$\rho_{i,j}^{n+1} = \rho_{i,j} - \frac{\delta t}{2\delta x}(\rho_{i+1,j}u_{i+\frac{1}{2},j}^{n+1} - \rho_{i-1,j}u_{i-\frac{1}{2},j}^{n+1})$$
$$- \frac{\delta t}{2\delta y}(\rho_{i,j+1}v_{i,j+\frac{1}{2}}^{n+1} - \rho_{i,j-1}v_{i,j-\frac{1}{2}}^{n+1}) - \frac{\delta t}{2}\rho_{i,j}D_{i,j}^{n+1}. \tag{2.6}$$

The quantity $D_{i,j}$ is the finite-difference form of $\nabla . \mathbf{u}$:

$$D_{i,j} = \frac{u_{i+\frac{1}{2},j} - u_{i-\frac{1}{2},j}}{\delta x} + \frac{v_{i,j+\frac{1}{2}} - v_{i,j-\frac{1}{2}}}{\delta y}.$$

The term proportional to $D_{i,j}$ is kept in (2.6) because $D_{i,j}$ is never exactly zero (in the numerical solution) and its retention is important for mass conservation.

If (2.6) is used with the ρ values on the right-hand side evaluated at time step n, a classical rapidly growing numerical instability will result. This instability is eliminated by requiring an iteration on the densities within each time step. Thus, a cycle of time advancement consists of first making a tentative guess for the new ρ values using equation (2.6) with n-level velocities and densities everywhere on the right-hand side. Then a new pressure field that makes $(\nabla . \mathbf{u})^{n+1}$ equal to zero is obtained by iteration. Finally, the densities are recalculated using equation (2.6) with the tentative new ρ values and the new velocities. If any cell density changes by more than some predetermined small percentage the sequence is repeated, calculating first a pressure field then new velocities, and again new densities. This iteration technique is extremely fast, requiring only very rarely

more than one extra pass through (2.6). No instability problems have been seen to arise in the use of this technique.

There is one subtle point regarding the numerical stability of the above finite-difference equations that needs further explanation. As was mentioned in connexion with the density equation (2.6), the use of density values at time level n in the convection terms leads to an instability. This instability is avoided by recalculating (2.6) at least once each time step, with the tentatively advanced values of density replacing the values previously at level n. Similarly, the use of values of quantities at time level n in the momentum convection terms in (2.1) and (2.2) makes these equations also unstable. Stability could be obtained, as it is in the density equation, by recalculating the velocities from (2.1) and (2.2) using the most updated values of velocities in the convection terms; however, this has not been attempted. Instead, stability is achieved, as in the original MAC method, by increasing the value of the viscosity. Increasing the viscosity compensates for a particularly undesirable kind of finite-difference truncation error, which gives a negative or anti-diffusion effect. If left unchecked these errors can enhance fluctuations to the point where they completely dominate a solution. To have a stable solution it has been shown (Hirt 1968) that the value of μ must exceed $\frac{1}{2}\delta t U_M^2$ and $\frac{1}{2}\delta x^2 U'_M$, where U_M is the maximum fluid speed and U'_M is the maximum absolute value of $\partial u/\partial x$.

The value of μ necessary to get a stable numerical solution is often much larger than the real value of μ for the fluid under study. In this situation it is necessary to exercise some caution if meaningful calculations are to be made. Two cases can be distinguished, according to whether the detailed effects of viscosity are of interest or not.

In cases where viscosity plays a relatively minor role, such as in the problem described in the next section, the effects of viscosity are to be minimized. If, in these cases, μ is chosen just large enough for stability and no larger, and if δt and δx values are chosen well within the characteristic time and space scales of the problem, then the influence of μ is not expected to be important.

On the other hand, in cases where the detailed effects of viscosity are important, as in a study of transition to turbulence, then the real value of μ must be used and the competing finite-difference errors must be made small relative to μ. In these cases it can be argued (see Hirt & Cook 1972), that the maximum Reynolds number accurately resolved by a mesh is less than N^2, where N is the number of mesh intervals spanning a characteristic problem dimension.

The program also includes a free-surface treatment that gives very smooth and accurate results. This treatment, which is considerably better than that used in the original MAC method, will not be discussed here as it is well described in the paper of Nichols & Hirt (1971).

It should be mentioned that values required at other than principal grid points are generally obtained by means of simple averages. The only exception to the above rule is in the convection terms, where we put

$$(\rho u^2)_{i,j} = \rho_{i,j} u_{i+\frac{1}{2},j} u_{i-\frac{1}{2},j}$$

and

$$(\rho v^2)_{i,j} = \rho_{i,j} v_{i,j+\frac{1}{2}} v_{i,j-\frac{1}{2}}.$$

Also, while the program allows for a variable viscosity, this feature was not used in the sample calculation which follows. Rigid-wall boundary conditions are considered to be either 'free-slip' (symmetry) or 'no-slip'. For the calculation in the next section the former boundary conditions were used.

3. Comparison of theory and experiment

Wu (1969), in a very nice tank experiment, measured the collapse of a uniformly mixed region in a linearly stratified fluid, and observed the internal wave pattern that resulted. In this section we discuss a numerical simulation of one of Wu's experimental configurations.

The experiment involved a volume of fluid confined in a rigid tank approximately 220 cm long and 120 cm high. The computing mesh covered the same region, cells having dimensions $\delta x = 5$ cm and $\delta y = 4$ cm. The time step, chosen for numerical stability and accuracy, was $\delta t = 0{\cdot}1$ s with $\mu = 0{\cdot}8$ g cm^{-1}s^{-1}. The initial radius (r_0) of the uniformly mixed circular region was taken to be 15·6 cm. The stratification was linear, and given by $\alpha = (-1/\rho_0)\,\partial\rho/\partial y = 0{\cdot}001$ cm^{-1} ($\rho_0 = 1$ g/c.c.), corresponding closely to one of the experimental values (0·0011 cm^{-1}). Both the experiment and the calculation were performed for only half of the problem for reasons of symmetry, see figure 1(*a*).

Since earlier calculations showed that a free surface did not significantly affect the internal wave dynamics we chose to ignore that option for the purpose of this paper and used a rigid upper boundary. Actually a simple argument shows that the change in free-surface elevation would be much less than 1 % of the initial radius of the uniform-density core.

A numerical simulation of a problem similar to that described above was attempted by Wessel (1969), also using a variant of the MAC method, and the Boussinesq approximation. However, his difference equations are not consistent and a highly questionable set of boundary conditions was used in their solution. He also used an initially square uniform-density region rather than the circular one used in the experiments. Although he claims agreement to within 15 % of the experimental data, his calculations must be regarded with suspicion without further supporting evidence.

The results of our calculations generally follow the observations of Wu, except that we do not follow the final collapse period owing to limitations of the numerical resolution that we chose. Also, the calculation does not show 'the wedge' that occurs at the tip of the expanding core before the final collapse stage for the same reason. We do, however, calculate the enlarged head of the tip that occurs at $t(\alpha g)^{\frac{1}{2}} \simeq 3$ in the experiment. Some of the results of the calculation are shown in figures 1(*a*)–(*g*). The horizontal dotted lines at $t = 0$ consist of massless Lagrangian particles and, as such, represent contours of constant density. These lines show the internal wave patterns in the same way as the layers of different coloured fluids used by Wu. The semicircular region half-way up the left boundary represents the uniformly mixed region with a constant density equal to that of the ambient fluid at the midpoint. Thus, the uniform-density region has neutral buoyancy.

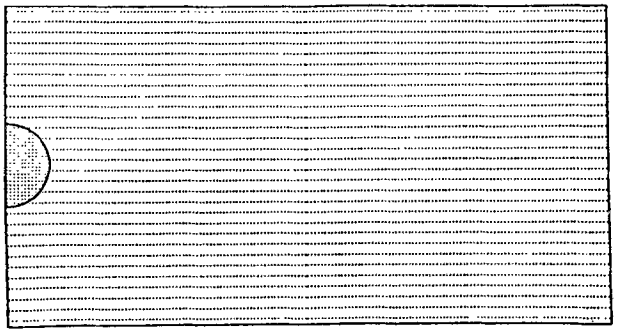

(*a*)

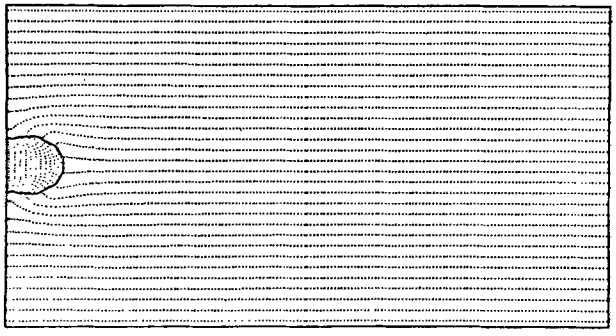

(*b*)

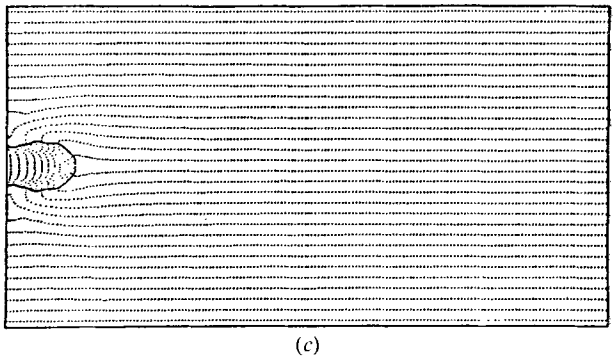

(*c*)

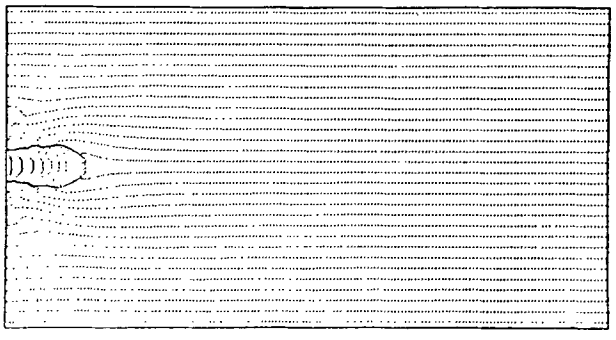

(*d*)

FIGURE 1. For legend see facing page.

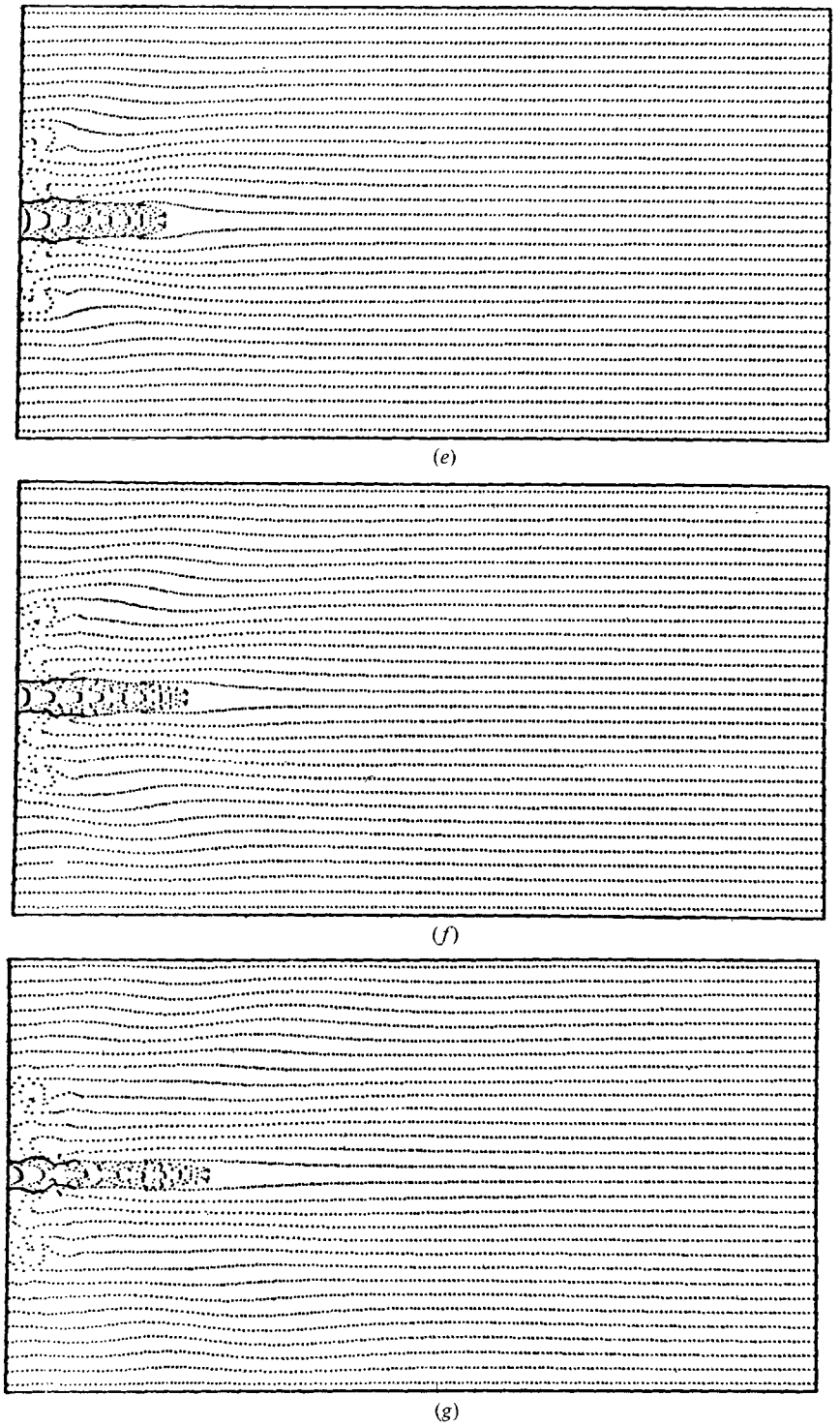

(*e*)

(*f*)

(*g*)

FIGURE 1. Marker-particle configurations at non-dimensional times (*a*) 0, (*b*) 2·0, (*c*) 3·0, (*d*) 4·0, (*e*) 7·0, (*f*) 10·0, (*g*) 15·0.

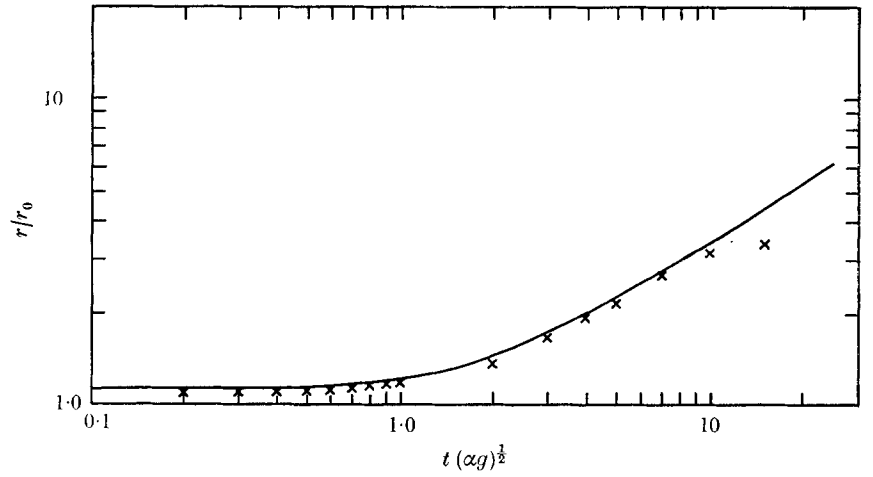

FIGURE 2. Comparison between theory and experiment for the horizontal length r/r_0 of the collapse region versus time. —, experiment; ×, calculated points.

From the plots of the Lagrangian particles one can construct a curve of maximum horizontal radius versus time. Such a curve is shown in figure 2 compared with a similar curve measured by Wu. While our results are slightly, but consistently, lower the agreement is within the experimental error up to when the vertical thickness of the collapsing region is comparable to a cell width. Once the core has collapsed to a thickness comparable to a cell size, the numerical solution is no longer accurate, which accounts for the slowdown of the calculated collapse after approximately $t(\alpha g)^{\frac{1}{2}} = 15$.

Figures 3(*a*)–(*d*) show plots of the velocity field suitably scaled for the graphs. Each line representing a velocity begins at a cell centre and thus it is easy to ascertain the velocity direction from the plot. It is interesting to note that Wu observed a change in scaling for core radius versus time depending on whether $t(\alpha g)^{\frac{1}{2}}$ was less than or greater than approximately 4. This change in scaling can be better seen by plotting $(r-r_0)/r_0$ with respect to $t(\alpha g)^{\frac{1}{2}}$, as in figure 4. The radius versus time curve is nicely approximated by three straight-line segments, with transitions between the different segments occurring near $t(\alpha g)^{\frac{1}{2}} = 2{\cdot}75$ and $t(\alpha g)^{\frac{1}{2}} = 6{\cdot}0$. A close look at the computed velocity fields in figures 3(*a*)–(*d*) reveals the origin of these transitions. While only a single eddy pair is observed during the initial stages of collapse, a second pair is clearly seen to be developing by $t(\alpha g)^{\frac{1}{2}} = 3{\cdot}0$ and a third pair by $t(\alpha g)^{\frac{1}{2}} = 7{\cdot}0$. Thus, the numerical results indicate that the flow remains self-similar as long as there is a particular distribution of eddies. However, with the addition of each new eddy pair a different self-similar scaling is required.

Although Wu did not observe a second transition in scaling behaviour this may be due to the fact that his reported results are the average obtained for a set of experiments covering more than an order-of-magnitude range in α. He did notice, however, that his data did follow a linear trend at early times when plotted with respect to $(r-r_0)/r_0$ as in figure 4.

The numerical results also indicate the mechanism that changes the shape of

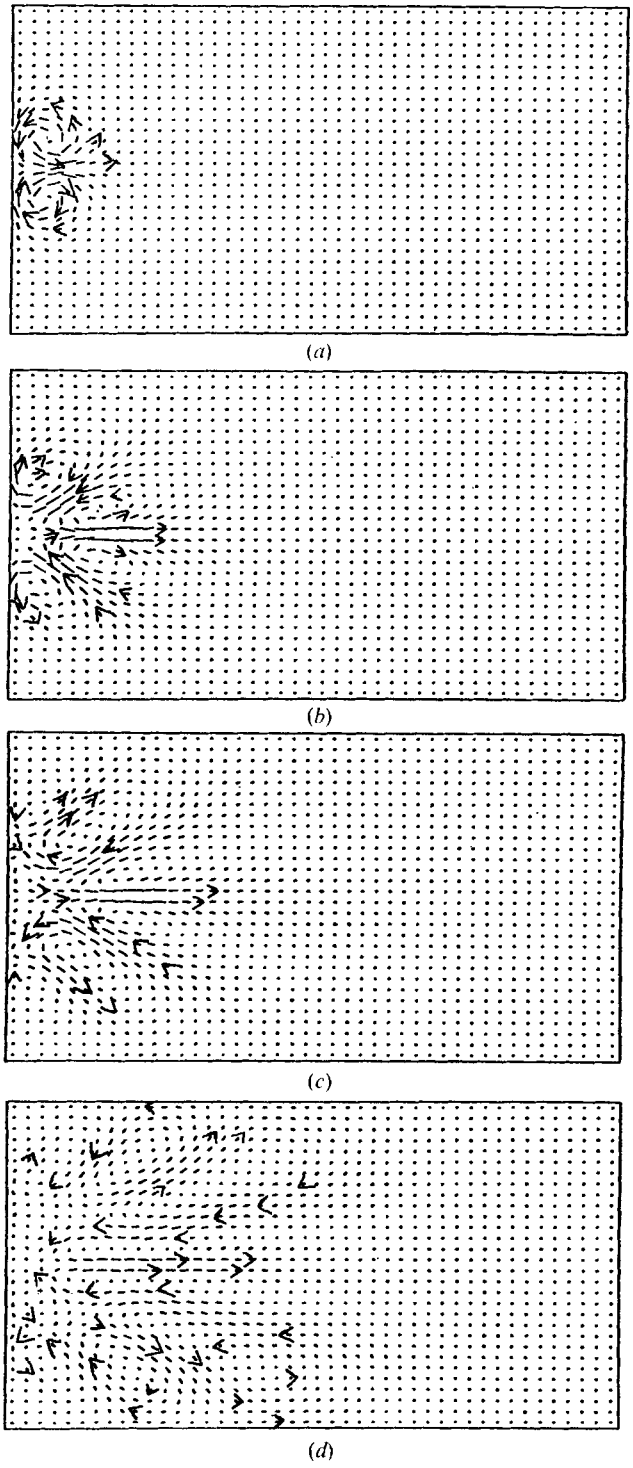

(*a*)

(*b*)

(*c*)

(*d*)

FIGURE 3. Velocity vector plots at non-dimensional times (*a*) 1·0, (*b*) 5·0, (*c*) 7·0, (*d*) 12·0.

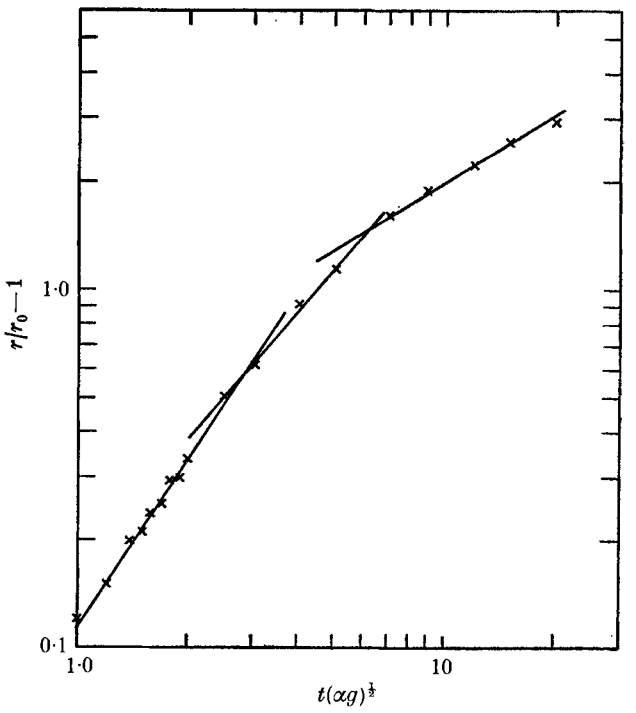

FIGURE 4. Plot of horizontal length $(r-r_0)/r_0$ versus time showing linear growth phases. Solid line segments approximate the numerical results, shown as crosses.

the tip of the expanding core. At times before the scaling transition at $t(\alpha g)^{\frac{1}{2}} = 4$, the tip is noticeably enlarged. After $t(\alpha g)^{\frac{1}{2}} = 4$ the enlargment disappears and the tip narrows into a sharp triangular point. This transition in shape results from a shift in the primary-eddy location. At early times the tip is to the right of the primary eddy and is therefore in a region of diverging flow, which causes it to expand. With the formation of secondary eddies the primary eddy is forced to the right of the tip, putting it in a region of converging flow. This causes the tip to narrow down, but a sharp point does not develop in the numerical solution because of insufficient resolution.

From the particle plots one can also observe the internal wave pattern, which agrees in structure with the one seen by Wu. More quantitatively, one can measure the angle between a line through the crests or troughs of the internal waves and a horizontal line through the top or bottom of the initial core region. A plot of this angle against the abscissa of the apex of the angle is shown in figure 5 compared with a curve representing the average of Wu's data. The agreement is seen to be quite satisfactory. The calculations, like the experimental data, show that the internal waves decay rapidly as they propagate away from the core centre. A film made from the computer plots clearly demonstrates the relationship between the phase and group velocities of the internal waves.

It should be mentioned that the wiggles that appear on the boundary of the collapsing region are of a numerical origin, probably related to the averaging of core and ambient densities in computational cells containing the core boundary.

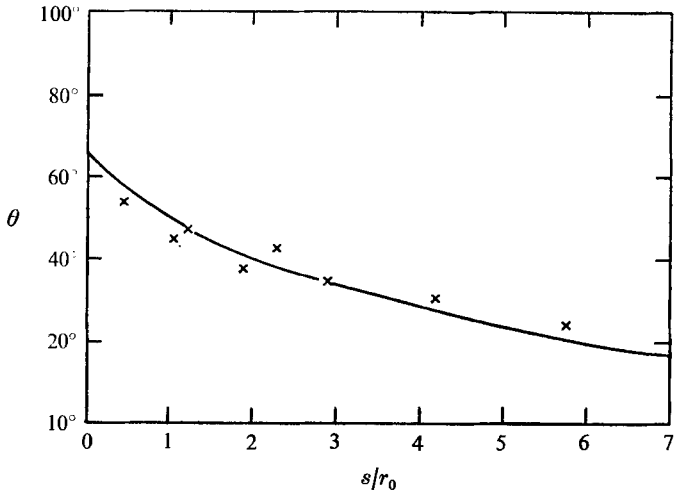

FIGURE 5. Comparison between theory and experiment of s, the abscissa of the intersection point of a line drawn through crests or troughs with a horizontal line through the top or bottom of the initial uniform density region, versus θ. —, average of the experimental points; ×, from calculation. The calculated points lie well within the experimental scatter.

The calculations referred to above were made on the CDC 7600 at the Los Alamos Scientific Laboratory. The time required for a single run was 5 min, which included sufficient plots for a film. Clearly, a much larger problem is easily feasible.

4. Conclusions

This numerical calculation of the collapse of a uniformly mixed region in a linearly stratified fluid agrees very well with available experimental data. As no special procedures were resorted to in obtaining this agreement, it may be concluded that the numerical solution method discussed in § 2 is a highly satisfactory one. With this in mind, it would be straightforward to study a host of related problems. For example, it would be possible to investigate the internal wave patterns produced when the density stratification is changed from linear to exponential, in which case the Brunt–Väisälä frequency would be constant, or to vary the initial uniform-density core from cylindrical to elliptical, or, by computing the entire left and right sides of the core, to include the effects of a variable horizontal current on the collapse structure. More complex phenomena can also be attacked with the SAPHIRE code, including situations where there are interactions between surface waves and internal waves, or where there are rectangular obstacles imbedded in the flow as was described in the original MAC method.

The authors wish to thank one referee for his stability analysis of the numerical method presented in this paper, and a second referee for several valuable criticisms. This work was supported in part by Science Applications, Inc., La Jolla, California, and in part by the United States Atomic Energy Commission.

REFERENCES

AMSDEN, A. A. & HARLOW, F. H. 1970 The SMAC method: a numerical technique for calculating incompressible fluid flows. *Los Alamos Sci. Lab. Rep.* LA-4370.

HARLOW, F. H. & WELCH, J. E. 1965 Numerical calculation of time-dependent viscous incompressible flow of fluid with free surface. *Phys. Fluids*, **8**, 2182.

HIRT, C. W. 1968 Heuristic stability theory for finite-difference equations. *J. Comp. Phys.* **2**, 339.

HIRT, C. W. & COOK, J. L. 1972 Calculating three-dimensional flows around structures and over rough terrain. *J. Comp. Phys.* to be published.

NICHOLS, B. D. & HIRT, C. W. 1971 Improved free surface boundary conditions for numerical incompressible flow calculations. *J. Comp. Phys.* **8**, 434.

WESSEL, R. W. 1969 Numerical study of the collapse of a perturbation in an infinite, density stratified fluid. *Phys. Fluids*, **12** (suppl.), II-171.

WU, J. 1969 Mixed region collapse with internal wave generation in a density-stratified medium, *J. Fluid Mech.* **35**, 531.